JMEPEG (2012) 21:406–410
DOI: 10.1007/s11665-011-9899-y

1059-9495/$19.00

In Situ Characterization of Pitting Corrosion of Stainless Steel by a Scanning Electrochemical Microscopy

C.F. Dong, H. Luo, K. Xiao, X.G. Li, and Y.F. Cheng

(Submitted May 25, 2010; in revised form December 13, 2011)

In this work, a scanning electrochemical microscopy (SECM) was used to characterize in situ the metastable and stable pitting processes occurring on a stainless steel in the chloride solution. It was found that metastable pitting would occur on the steel that was at corrosion potential and passive potential. The positive shift of potential would enhance the metastable pitting current. On application of a potential exceeding pitting potential, the pit became stabilized and maintained a continuous growth. The SECM is capable of detecting the microdissolution event and provides a "visual" observation of the pitting processes.

Keywords pitting corrosion, scanning electrochemical microscopy, stainless steel

1. Introduction

Pitting corrosion usually occurs on metals that are passivated in the service environments. Conventional electrochemical measurement techniques including potentiodynamic polarization curve, cyclic polarization, and electrochemical impedance spectroscopy (EIS) have been used to study pitting corrosion of metals (Ref 1-3). However, these techniques are incapable of monitoring in situ the pitting processes and characterizing the initiation and growth stages of a corrosion pit. Since corrosion pits are usually initiated at microscopic sites, a direct "visualization" of the various stages a corrosion pit experiences will be essential to understand the mechanism of pitting corrosion. Scanning electrochemical microscopy (SECM) technique provides a promising approach to monitor pitting (Ref 4-6).

The dissolution and passivity of iron (Ref 7, 8) and localized corrosion of stainless steels (Ref 9, 10) have been investigated by SECM. For example, González-García et al. (Ref 11) used SECM to detect and map the metastable pits as well as the surrounding cathodic reaction on a 304 stainless steel at corrosion potential. The anodic oxidation of the passive film was detected during propagation of pits. Zhu and Williams (Ref 12) observed the evolution of metastable pits adjacent to sulfide inclusions on a stainless steel by SECM when the electrode was polarized to high potentials, and suggested that the electrochemical activity was enhanced around the sites of the inclusions compared to other areas. Casillas et al. (Ref 13-15) used SECM to detect the precursor states of pitting on titanium. Moreover, the SECM has been used extensively on various aluminum (Al) alloys to study their pitting behavior. For example, Davoodi et al. (Ref 16) combined SECM with electrochemical atomic force microscopy to demonstrate the ongoing localized dissolution related to intermetallic particles in the Al alloys, which may occur well below the breakdown potential. Simões et al. (Ref 17) used SECM to investigate the processes occurring at the surface of exposed metal when electrically connected or disconnected in a galvanic couple with the Mg-rich coating. The SECM allowed indirect sensing of the cathodic activity above the electrodes, where the cathodic protection provided by magnesium to Al substrates acts by both preventing pit nucleation and inhibiting the growth of the pre-existing pits.

In this work, pitting corrosion of an AISI 2205 stainless steel was studied by SECM in a chloride solution. The dissolution current generated from pitting was detected, and the pitting processes were monitored in situ.

2. Experimental

Specimens used in this work were cut from a sheet of 2205 stainless steel supplied by Avesta Inc., with a chemical composition (wt.%): C 0.014, Cr 22.39, Ni 5.68, N 0.17, Mo 3.13, Si 0.39, Mn 1.38, S 0.001, P 0.023, and Fe balance. In order to homogenize the microstructure of the steel, the specimens were heated at 1100 °C for 2 h under atmosphere, and then cooled in furnace. It is realized that the heat treatment on alloys would result in a phase separation, which causes the separated anodic and cathodic sites during corrosion of the alloys. The microstructural homogenization was conducted in this work in order to remove the effect of the phase separation on pitting process, and focused the investigation on determination of the role of potential in the pitting occurrence. The next step of this research will utilize alloys used in service as the targets for the pitting characterization.

The specimens were machined into 0.5-mm diameter cylinders with a 5 mm height. After sealing in a LECO epoxy, the electrodes were ground consecutively from 600 to 2000 grit SiC paper, polished to 0.1 μm alumina paste, and cleaned ultrasonically with ethanol.

C.F. Dong, H. Luo, K. Xiao, and **X.G. Li**, Corrosion and Protection Center, University of Science and Technology Beijing, Beijing 100083, China; and **Y.F. Cheng**, Department of Mechanical & Manufacturing Engineering, University of Calgary, Calgary, AB T2N 1N4, Canada. Contact e-mails: dongchf@hotmail.com and fcheng@ucalgary.ca.

The test solution contained 0.1 M NaCl, which was prepared from reagent grade chemicals and distilled water. Prior to test, the solution was purged with a high-purity nitrogen gas (99.99%) for 1 h. All tests were performed at ambient temperature (22 °C) and open to air.

The potentiodynamic polarization measurement was performed on a three-electrode cell, with the stainless steel electrode as working electrode, a platinum plate as counter electrode, and a saturated calomel electrode (SCE) as reference electrode. The measurement was carried out using a Model 273A potentiostat/galvanostat (EG&G) with a potential scan rate of 0.333 mV/s.

The SECM test was carried out through a M370 scanning electrochemical workstation, as schematically shown in Fig. 1. The SECM imaging was performed using a Pt microelectrode probe with a 10 μm tip. The lateral resolution of SECM depends on the tip size, the electrode-probe distance, and the electrolyte conductivity. Before test, a calibrating curve was measured in a solution containing I^-/I_3^- as a redox couple. An optimal 10 μm of the distance between Pt microelectrode and the steel electrode was determined. During test, the electrode was held either at corrosion potential or an anodically polarized potential. The potential of the Pt probe was kept at 600 mV(SCE), which was the characteristic potential to oxidize Fe, rather than Cr, Ni, and other elements in the steel (Ref 11).

3. Results and Discussion

The potentiodynamic polarization curve measured on the stainless steel electrode in 0.1 M NaCl solution is shown in Fig. 2. It is seen that the electrode would be passivated in the solution, with a corrosion potential (E_{corr}) of −340 mV(SCE) and a passive potential region up to approximately 500 mV(SCE). The current density increased rapidly after the potential exceeded the pitting potential (E_{pit}) of about 500 mV(SCE).

Three potential points were selected for SECM tests, i.e., E_{corr}, 0.05 and 1.4 V(SCE), as marked as points A, B, and C in Fig. 2, which represented the typical potentials where the steel was at free corrosion, passivity, and pitting corrosion, respectively.

Figure 3 shows the SECM images measured on the steel electrode that was at E_{corr} immediately and after 10 min of immersion in 0.1 M NaCl solution. A few anodic current peaks <20 pA were observed when the electrode was immersed in the solution. When the immersion time increased to 10 min, the value of the background current decreased slightly. For example, the background currents in Fig. 3(a) and (b) were approximately 6 and 2 pA, respectively, indicating the self-passivation of stainless steel in the solution. The anodic current peaks are due to the local dissolution of some active spots, such as inclusions, on the steel surface. The position of the current peaks changed with time, with some formerly formed peaks in Fig. 3(a) disappearing and some new peaks generating (Fig. 3b), showing the metastable nature of the local dissolution activity.

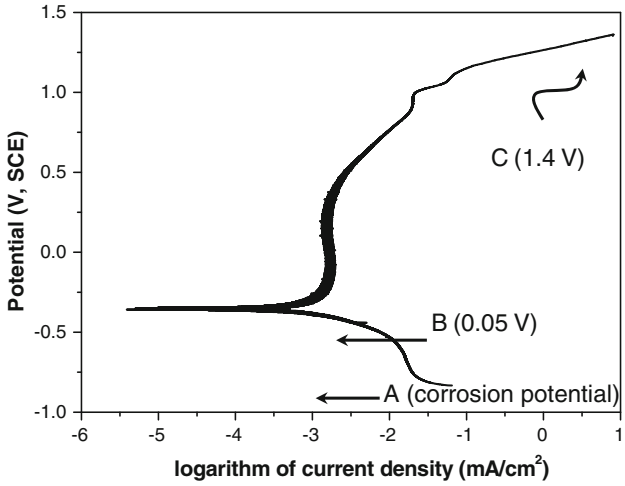

Fig. 2 Potentiodynamic polarization curves of the stainless steel electrode in 0.1 M NaCl solution

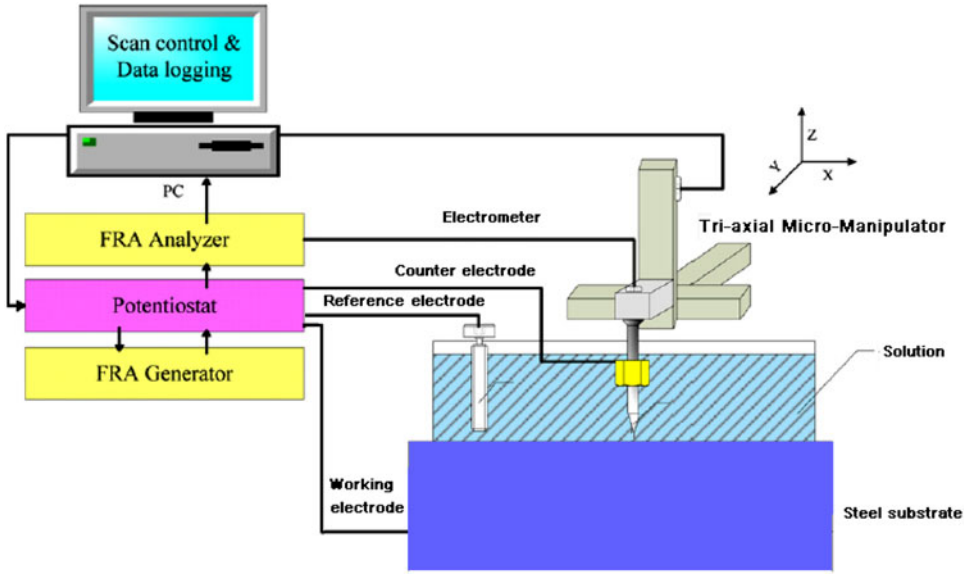

Fig. 1 Schematic diagram of the experimental setup for the SECM measurements

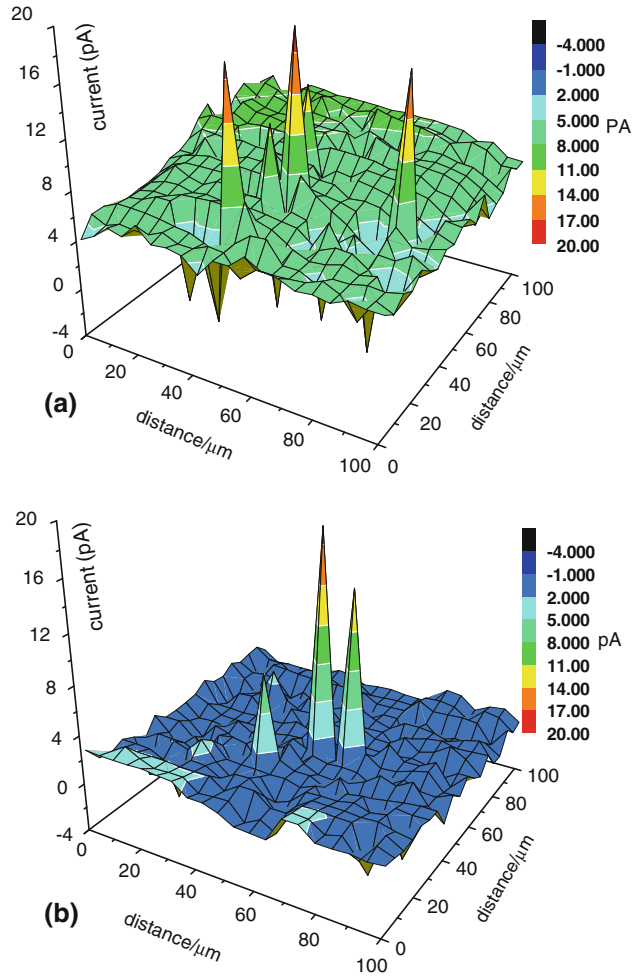

Fig. 3 SECM images measured on the steel electrode at corrosion potential immediately (a) and after 10 min (b) of immersion in 0.1 M NaCl solution

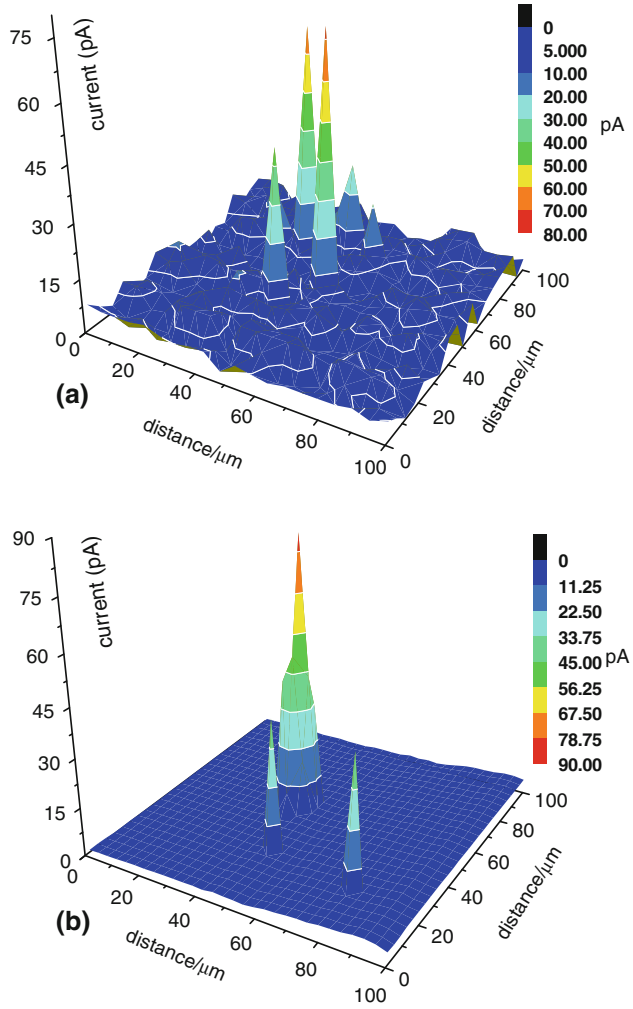

Fig. 4 SECM images measured on the steel electrode at 0.05 V(SCE) immediately (a) and after 10 min (b) of immersion in 0.1 M NaCl solution

Figure 4 shows the SECM images measured on the steel electrode that was at 0.05 V(SCE) immediately and after 10 min of immersion in 0.1 M NaCl solution. It is seen that, with a background current of about 5 pA, the local anodic current peaks could be up to 70 pA immediately when the electrode was immersed in the solution. With the increase of the immersion time, the background current decreased, while the peak current increased to about 90 pA. The results show that, while the steel is passivated at the passive potential, the local dissolution of the active spots increases compared to that at E_{corr}. Thus, the metastable pitting is enhanced with potential, even at the passive range.

Figure 5 shows the SECM images measured on the steel electrode that was at 1.4 V(SCE) after various times of immersion in 0.1 M NaCl solution. Quite high background current of about 50 nA and anodic current peak up to 140 nA were observed when the electrode was immersed in the solution (Fig. 5a). After 3 min of immersion, the background current and peak current further increased. When the polarization time exceeded 10 min, the background current and peak current reached the μA magnitude. A sharp current rise was observed at this stage.

In general, pitting corrosion of metals experiences three stages—initiation, metastable pitting, and stable pitting growth. During the pit initiation, the passive film is attacked by aggressive species such as chloride ions existing in the environment. The breakdown of the film usually occurs at sites, where the film is relatively weak. Various microdefects and nonmetallic inclusions in the steel result in high local dissolution activities, becoming the potential sites for initiation of pits. When the pit stabilization criterion has not been met, these pits are metastable and will be repassivated in the environment (Ref 18). This study demonstrates that metastable pitting would occur at corrosion potential and passive potential. With the increase of the test time, the formerly formed current peaks disappear, showing that the metastable pits are passivated. The newly generated peaks are associated with new metastable pits. Since the applied potential is at E_{corr} or a passive potential, the resulting dissolution current is not sufficient to cause the transition of metastable pits toward stabilization.

When the potential is shifted to 1.4 V(SCE), which is more positive than E_{pit}, both the background current and the peak current increase remarkably. In particular, the peak current increases continuously with time (Fig. 5), indicating that the pit becomes stable, and maintains a continuous growth.

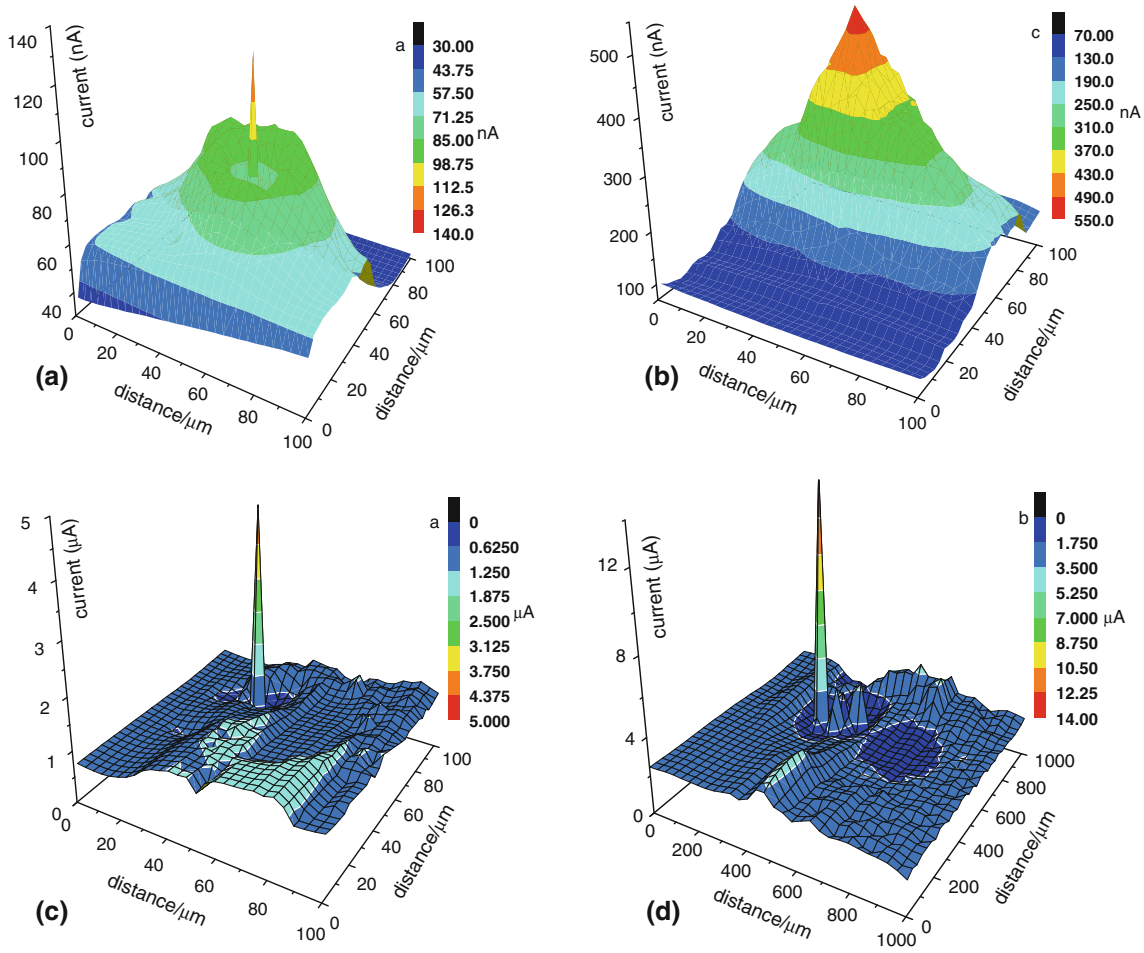

Fig. 5 SECM images measured on the steel electrode at 1.4 V(SCE) immediately (a) and after 3 min (b), 10 min (c) and 20 min (d) of immersion in 0.1 M NaCl solution

4. Conclusions

The SECM is capable of characterizing in situ the metastable and stable pitting occurring on stainless steel. Metastable pitting would at corrosion potential and passive potential. The dissolution current generated during metastable pitting is not sufficient to cause the transition of metastable pits toward stabilization. On application of a potential exceeding pitting potential, the pit becomes stabilized and maintains a continuous growth.

Acknowledgments

This work is supported by the National Program for Basic Conditions Platform (No. 2005DKA10400) and Canada Research Chairs Program.

References

1. A.J. Invernizzi, E. Sivieri, and S.P. Trasatti, Corrosion Behavior of Duplex Stainless Steels in Organic Acid Aqueous Solutions, *Mater. Sci. Eng. A*, 2008, **485**, p 234–242
2. M. Martinsa and L.C. Casteletti, Microstructural Characteristics and Corrosion Behavior of a Super Duplex Stainless Steel Casting, *Mater. Charact.*, 2009, **60**, p 150–155
3. I.H. Lo and W.-T. Tsai, Effect of Selective Dissolution on Fatigue Crack Initiation in 2205 Duplex Stainless Steel, *Corros. Sci.*, 2007, **49**, p 1847–1861
4. T.E. Lister, P.J. Pinhero, T.L. Trowbridge, and R.E. Mizia, Localized Attack of a Two-Phase Metal, Scanning Electrochemical Microscopy Studies of NiCrMoGd Alloys, *J. Electroanal. Chem.*, 2005, **597**, p 291–298
5. I. Annergren, F. Zou, and D. Thierry, Application of Localized Electrochemical Techniques to Study Kinetics of Initiation and Propagation During Pit Growth, *Electrochim. Acta*, 1999, **44**, p 4383–4393
6. M. Etienne, A. Schulte, and W. Schuhmann, High resolution Constant-Distance Mode Alternating Current Scanning Electrochemical Microscopy (AC-SECM), *Electrochem. Commun.*, 2004, **6**, p 288–293
7. K. Fushimi and M. Seo, An SECM Observation of Dissolution Distribution of Ferrous or Ferric Ion From a Polycrystalline Iron Electrode, *Electrochim. Acta*, 2001, **47**, p 121–127
8. Y.-F. Yang and G. Denuault, Scanning Electrochemical Microscopy (SECM): Study of the Formation and Reduction of Oxides on Platinum Electrode Surfaces in Na_2SO_4 solution (pH = 7), *J. Electroanal. Chem.*, 1998, **443**, p 273–282
9. H. Tanabe, K. Togashi, U.K. Mudali, and T. Misawa, In situ pH Measurements During Localized Corrosion of Type 316LN Stainless Steel Using Scanning Electrochemical Microscopy, *J. Mater. Sci. Lett.*, 1998, **17**, p 551–553
10. C.H. Paik, H.S. White, and R.C. Alkire, Scanning Electrochemical Microscopy Detection of Dissolved Sulfur Species From Inclusions in Stainless Steel, *J. Electrochem. Soc.*, 2000, **147**, p 4120–4124
11. Y. González-García, G.T. Burstein, S. González, and R.M. Souto, Imaging Metastable Pits on Austenitic Stainless Steel In Situ at the

Open-Circuit Corrosion Potential, *Electrochem. Commun.*, 2004, **6**, p 637–642
12. Y. Zhu and D.E. Williams, Scanning Electrochemical Microscopic Observation of a Precursor State to Pitting Corrosion of Stainless Steel, *J. Electrochem. Soc.*, 1997, **144**, p L43–L45
13. N. Casillas, S.J. Charlebois, W.S. Smyrl, and H.S. White, Scanning Electrochemical Microscopy of Precursor Sites for Pitting Corrosion on Titanium, *J. Electrochem. Soc.*, 1993, **140**, p L142–L145
14. N. Casillas, S.J. Charlebois, W.S. Smyrl, and H.S. White, Pitting Corrosion of Titanium, *J. Electrochem. Soc.*, 1994, **141**, p 636–642
15. P. James, N. Casillas, and W.S. Smyrl, Simultaneous Scanning Electrochemical and Photoelectrochemical Microscopy by Use of a Metallized Optical Fiber, *J. Electrochem. Soc.*, 1996, **143**, p 3853–3865
16. A. Davoodi, J. Pan, C. Leygraf, and S. Norgren, In Situ Investigation of Localized Corrosion of Aluminum Alloys in Chloride Solution Using Integrated EC-AFM/SECM Techniques, *Electrochem. Solid State Lett.*, 2005, **8**, p B21–B24
17. A.M. Simões, D. Battocchi, D.E. Tallman, and G.P. Bierwagen, SVET and SECM Imaging of Cathodic Protection of Aluminium by a Mg-Rich Coating, *Corros. Sci.*, 2007, **49**, p 3838–3849
18. Y.F. Cheng, M. Wilmott, and J.L. Luo, Transition Criterion of Metastable Pitting Towards Stability for Carbon Steel in Chloride Solutions, *Br. Corros. J.*, 1999, **34**, p 280–284